Analyst

PAPER

View Article Online
View Journal

Cite this: DOI: 10.1039/d6an00119j

Separating *O*-desmethylvenlafaxine and tramadol enantiomers using two-dimensional chiral LC × DMS mass spectrometry

A. Dawson McLachlan, †[a] Rashne Vakharia,†[a,b] Emir Nazdrajić, [a] Diana M. Cárdenas-Soracá, [b] Leslie M. Bragg, [b] Mark R. Servos [b] and W. Scott Hopkins *[a,c]

Tandem mass spectrometry relies on unique parent-to-product transitions for selective analysis. For sets of isomers or isobars that have identical behaviors in multiple separation dimensions (*e.g.*, LC retention, *m*/*z*), quantitation is challenging owing to feature convolution. For example, recent environmental analysis of the enantiomers of *O*-desmethylvenlafaxine (ODV), an anti-depressant manufactured in a racemic mixture, identified tramadol (TRA, a racemic painkiller) as a co-eluting interference. Here, we demonstrate that differential ion mobility spectrometry (DMS) coupled with chiral LC-MS^2 can be used to separate and quantify the enantiomers of ODV and TRA. This method was applied to six wastewater influent samples from an Ontario municipal wastewater plant, where the sum of the enantiomeric concentrations was statistically identical to the racemic concentrations observed on reverse-phase LC-MS^2 (t-test, α = 0.05, *p*-value = 0.26 for ODV and *p*-value = 0.47 for TRA). We also identify low-intensity product ions specific to ODV that enable isolation and quantitation *via* chiral LC-MS^2 alone, albeit at a relatively high limit of quantitation (LOQ) in comparison to the most intense MRM transition (*m*/*z* 264 → 58). Using our chiral (LC × DMS)-MS^2 method, the instrumental LOQ of each enantiomer of TRA was determined to be 0.67 ng mL^{-1} and 5.0 ng mL^{-1} for the enantiomers of ODV.

Received 30th January 2026,
Accepted 4th March 2026

DOI: 10.1039/d6an00119j

rsc.li/analyst

1. Introduction

The presence of pharmaceutically active compounds in the environment has become a subject of concern.[1,2] The high usage of prescription pharmaceuticals, combined with poor biological metabolism for many of these compounds and their relatively low removal efficiency during wastewater treatment has led to relatively high environmental concentrations in some urban areas.[2] Constant exposure of aquatic life to polluted waters can lead to the bioaccumulation of some of these compounds, which can then persist and represent a risk.[3,4] Despite many of these pharmaceuticals being sold as racemic mixtures, very few environmental studies have included analysis for the specific enantiomers.[5] Whether bioaccumulation and the biological effects in aquatic life associated with pharmaceuticals found in the environment are enantiomerically specific is an interesting open question, and environmental studies must first be established before addressing this.[6]

ODV is a prescription anti-depressant, that is also one of the human metabolites of venlafaxine, another chiral anti-depressant.[7] Both venlafaxine and ODV have been associated with developmental toxicity (among other biological effects) in fish.[8–10] ODV, which has one chiral centre, is synthesized racemically as (*S*)-ODV and (*R*)-ODV. Likewise, *cis*-TRA (hereafter TRA) is a chiral synthetic opioid that can be prescribed as a painkiller.[11,12] TRA has two chiral centres and the (*R*,*R*) and (*S*,*S*) enantiomers are produced racemically during synthesis. Conventional analysis of trace enantiomeric environmental contaminants employs chiral liquid chromatography tandem mass spectrometry LC-MS^2 and sometimes involves preconcentration *via* solid phase extraction.[13–15] Preconcentration is required if more sensitive limits of detection (LOD) or limits of quantitation (LOQ) are desired. The chiral stationary phase (*e.g.*, vancomycin in the Agilent InfinityLab Poroshell 120 Chiral-V column) promotes enantioselective interactions with one enantiomer present in the racemic mixture.[14] The presence of interfering species in LC-MS^2, *i.e.*, compounds that have similar behaviours in

[a]*Department of Chemistry, Faculty of Science, University of Waterloo, Ontario, Canada. E-mail: shopkins@uwaterloo.ca*
[b]*Department of Biology, Faculty of Science, University of Waterloo, Ontario, Canada*
[c]*WaterFEL Free Electron Laser Laboratory, University of Waterloo, Waterloo, Ontario, Canada*
† Contributed equally to this work.

each separation dimension, can result in erroneous quantitation. For example, when compounds that co-elute in the chromatographic dimension exhibit identical precursor mass-to-charge (m/z) and product ion m/z, inaccurate quantitation of the targeted analyte can occur. ODV and TRA are isomers with chemical formula $C_{16}H_{25}NO_2$ and are an example of such an interfering analyte pair.

In their recent investigation of pharmaceutical bioaccumulation in rainbow darters (*Etheostoma caeruleum*; a species of small freshwater fish), Kowalczyk reported a chiral LC method for targeted analysis of several chiral pharmaceuticals, including ODV.[16] During the analysis of (*S*)-ODV, Kowalczyk observed a co-eluting interference that they later identified as (*R*,*R*)-TRA *via* reference standard.[16] Differentiation between the signals of (*S*)-ODV and (*R*,*R*)-TRA would enable exploration of the environmental concentrations and bioaccumulation of specific ODV and TRA enantiomers in aquatic life. For separating chiral species, liquid chromatography using a chiral column is the most common method.[6,17,18] There are three methods by which isomers are commonly differentiated: (1) unique multiple reaction monitoring (MRM) transitions for species that exhibit distinct product ions, (2) ion mobility spectrometry (IMS) for species exhibiting collision cross sections that differ by more than ~2%, and (3) liquid chromatography for species with significantly different retention times such that they do not co-elute.[19]

The use of ion mobility spectrometry to separate or filter isomers has been explored extensively.[20,21] Differential mobility spectrometry (DMS) is an IMS technique capable of separating sets of structural isomers,[19,22] including prototropic isomers (*i.e.*, protomers),[20,23] pharmaceutical compounds, cannabinoids,[21,23,24] and peptides.[25] The DMS cell consists of two parallel electrode plates, between which ions pass while an asymmetric and oscillating electric field (waveform) is applied. This waveform, known as the separation voltage (SV), accelerates and decelerates ions leading to a cycle of ion heating/cooling with each duty cycle. Because the mobility of an ion under high-field conditions is not linearly proportional to the low-field mobility, the SV drives migration of the ion off the transmission axis.[22] To correct the ion's trajectory, a static potential known as the compensation voltage (CV) is applied. The CV required for transmission of an ion through the DMS cell when a particular SV is applied is dependent on that ion's differential mobility. Since isomers have slightly different sizes and can interact differently with the gaseous environment, they exhibit different differential mobilities and, given sufficient difference, may be spatially separated.[22] In some cases, differential mobility can be enhanced by introducing a low vapor pressure of solvent to the carrier gas, thereby modifying the collision environment and introducing chemical specificity *via* dynamic ion-solvent clustering.[21,26,27] Typical modifier solvents include acetonitrile (ACN), ethyl acetate (EtAc), isopropanol (IPA), and acetone (ACE). By changing the solvent modifier, one changes the chemical interactions experienced by the analyte ions during transmission and effectively tunes the ion-solvent clustering behaviour and distribution within the DMS cell.

Ion behaviour within the DMS cell is typically classified as one of three common types. Strong dynamic clustering in DMS, or Type A dispersion behaviour, is characterized by the need for a decreasing CV for optimal ion transmission as SV increases.[22] This implies that ion-solvent clusters form under low-field (*i.e.*, cold) conditions and evaporate during the high-field portion of the waveform.[22] For some analyte ions in some modified environments, there is a SV at which the CV stops its decreasing trend and begins increasing with increasing SV. This behaviour, known as Type B dispersion, is indicative of weak dynamic clustering; dynamic clustering/de-clustering can occur at low SV, but at high SV, ions experience such high heating under high-field conditions that they no longer cluster under low-field conditions.[22] Type C dispersion, characterized by increasing CV with increasing SV, is indicative of hard-sphere collision conditions wherein ion-solvent cluster formation is thermodynamically unfavorable.[22]

DMS separation of enantiomeric species has been reported, but requires derivatization of the analyte, which can be challenging for trace analysis.[28] Jin and co-workers demonstrated derivatization and separation of allopregnanolone, prenanolone, and their 3β epimers, *via* a hybrid LC and DMS method, which was also successful for reducing chemical noise and isobaric interferences.[28,29] More recently, Jacquet *et al.*, Ekmekciu *et al.* and Ryan *et al.* reported the application of DMS and LC in hybrid two-dimensional LC × DMS-MS^2 workflows,[30–32] and modifications to this approach have been integrated in targeted methodologies.[33] The separation of ODV and TRA *via* IMS was attempted by Werres *et al.* who reported that protonated ODV and TRA are only partially resolved using travelling wave IMS (TWIMS), DMS, and a differential mass analyzer.[19] In their work, they found that DMS offered the best separation, though still insufficient for baseline resolution of the isomers.[19]

In this work, we demonstrate two-dimensional chiral LC × DMS-MS^2 to differentiate the enantiomers of protonated ODV and TRA. Further, we report ion-solvent binding energies, which we computed to garner further insights regarding the isomer separation achieved using DMS. Additionally, collision cross-section (CCS) measurements of ODV and TRA were obtained using TWIMS. We also identify collision induced dissociation (CID) conditions that yield unique MRM transitions for ODV, which can be used to distinguish ODV from TRA, albeit at the cost of sensitivity. To test the two-dimensional chiral LC × DMS-MS^2 method, we analyse influent of municipal wastewater collected at a treatment facility in Ontario, Canada, and assess analytical separation and quantitation of both ODV and TRA. This proof-of-concept work can be extended to the quantitation of other chiral analytes in complex mixtures, such as biological tissues and fluids, enabling evaluation of, for example, enantiomeric bioaccumulation.

2. Experimental

2.1 Chemicals

Analytical reference standards of ODV and TRA, along with the isotopically labelled TRA^{13}C-D$_3$ and ODV-D$_6$ used as internal standards were purchased from MilliporeSigma Canada Ltd (Oakville, ON, Canada). All HPLC-grade solvents, including isopropanol (IPA), acetonitrile (ACN), ethyl acetate (EtAc), acetone (ACE), methanol (MeOH), and ethanol (EtOH) were purchased from MilliporeSigma Canada Ltd. Formic acid and acetic acid were also purchased from MilliporeSigma. Ammonium acetate was purchased from VWR (Mississauga, ON, Canada). Waters Major Mix for TWIMS CCS calibration was purchased from Waters Corporation (Milford, MA, USA).

For sample preparation, LC-MS-grade MeOH, ACN, and formic acid (FA) were obtained from Fisher Scientific International Inc. (Missisauga, ON, Canada). LC-grade ammonium formate was purchased from Millipore Sigma Canada Ltd, along with the Milli-Q Advantage A10 water purification system which was used to produce Milli-Q water.

2.2 LC- and DMS-MS experiments

All column information and reverse-phase liquid chromatography methods are provided in Table S1, and MS source conditions are provided in Table S2. All analysis was performed on an Agilent 1100 high-performance liquid chromatography (HPLC) system connected to a triple-quadrupole mass spectrometer (QTRAP 5500, SCIEX, Concord, ON, Canada) *via* an electrospray ionization source and analyzed in positive ion mode. For experiments using the linear ion trap (LIT), the enhanced product ion (EPI) scan mode was used. If DMS was being used, the SelexIon DMS device (SCIEX, Concord, ON, Canada) was installed between the TurboV source and QTRAP 5500s MS orifice. An overview schematic of the experimental set-up is presented in Fig. S1. For DMS experiments employing solvent modifier, the N_2 carrier gas was entrained with 1.5 mol% of HPLC-grade solvent modifier (IPA, MeOH, ACN, EtAc, and ACE). N_2 gas opposing the transmission of ions, known as the resolving gas (DR), was used for some separation experiments involving solvent modifiers. DR flow opposes carrier gas flow (and thus ion transmission) resulting in analyte ions being exposed to more DMS duty cycles, leading to narrower peaks (in CV-space) and increased resolution, albeit at the loss of ion signal intensity.

For all DMS experiments, dispersion plots were generated by increasing the separation voltage (SV) and monitoring the compensation voltage (CV) required for transmission into the MS. When employing the optimal SV for separation, CV was scanned across the appropriate range for transmission of ODV and TRA at multiple chromatographic retention times encompassing the analyte LC elution profile.

2.3 TWIMS-MS experiments

A Waters Synapt G2-Si HDMS mass spectrometer (Waters Corporation, Milford, MA, USA) equipped with a T-Wave cell was used to measure the CCSs of ODV and TRA. The instrument was set to positive ionization mode with an m/z acquisition of 50–1200 and mass calibrated using sodium formate. The CCS calibration curves were generated by plotting the arrival time distribution of calibrant m/z observed in the Waters Major Mix (see Fig. S2) with T-Wave wave height settings of 36 V, 38 V, and 40 V while maintaining a wave velocity of 700 m s^{-1}. The T-Wave conditions were then used to determine the arrival time distributions of ODV and TRA *via* infusion of 200 ng mL^{-1} standards, followed by a mixture to determine whether features could be resolved at these conditions. The source parameters were as follows: capillary voltage = 2.5 kV; sampling cone = 40 V; source offset = 80 V; source temperature = 140 °C; cone gas flow = 50 L h^{-1}; desolvation gas flow = 600 L h^{-1}; desolvation temperature = 400 °C; and nebulizer gas pressure = 6.5 bar.

2.4 Sample preparation *via* solid phase extraction (SPE)

Solid-phase extraction (SPE) was performed on 24 h composites of influent collected from an Ontario municipal wastewater treatment plant (WWTP). Water samples were extracted using a previously optimized method developed by Cárdenas-Soracá *et al.* using Bond Elut NEXUS WCX (6 mL, 150 mg, 70 μm) cartridges obtained from Agilent Technologies (Mississauga, ON, Canada).[34] Briefly 50 mL raw influent wastewater samples were acidified, spiked with 100 μL of a 500 ng mL^{-1} internal standard mixture (including ODV-D$_6$ and TRA^{13}C-D$_3$) and loaded onto WCX cartridges preconditioned with methanol and 1% formic acid. Afterwards cartridges were rinsed with 5 mL of 5% MeOH in Milli-Q water and dried under vacuum for approximately 15 minutes. Cartridges were eluted with 4 mL and then 3 mL of 5 M FA in 1 : 1 MeOH : ACN, followed by 2 mL of MeOH. Finally, the eluent was evaporated to dryness under nitrogen and reconstituted in 0.5 mL of 2.5 mM ammonium formate in 9 : 1 H_2O : MeOH + 0.1% FA. Samples were stored at −20 °C prior to analysis using LC-MS and LC × DMS-MS^2.

2.5 Computational analysis

Electronic structure calculations were performed to explore gas-phase ion-solvent clusters containing ODV and TRA with IPA. Structural inputs were first generated in GaussView 6.0.16 before conformer filtering. Conformer candidate structures for the bare and clustered ions were generated by CREST version 2.12 with xTB version 6.4.0.[35] The geometries of unique bare ion and ion-solvent clusters were then refined at the DFT ωB97X-D3BJ/def2-TZVPP level of theory,[36–44] which more accurately maps the potential energy surface of the cluster. For the DFT-optimized structures, electronic energies were improved *via* DLPNO-CCSD(T)/def2-TZVPP calculations. CCS values of the ions and ion-solvent clusters were generated using MobCal-MPI 2.0.[45–47] All calculations were performed using the ORCA 6.0.0 suite of programs.[48–51] Thermochemical corrections acquired following normal mode analysis enabled Boltzmann-weighting of conformers and clusters present in the gas-phase ensembles; these relative populations were then employed to describe the effective CCS of the ensemble.[45] The

Boltzmann-weighting process was performed by the Pythonic Orca Data Processing and Analysis Libraries (PodPals) GUI.[52]

3. Results and discussion

3.1. MS-only analysis

ODV and TRA are structural isomers, with similar fragmentation products. In positive ionization mode MS, the protonated parent molecules exhibit *m/z* 264 and two major MRM transitions associated with loss of H_2O (*m/z* 264 → 246) and formation of $(CH_3)_2N^+(CH_2)$ (*m/z* 264 → 58). *Via* direct infusion, the MS^2 spectrum of each analyte was collected (see Fig. S3). Using the enhanced product ion (EPI) scan mode, we identified three product ions of ODV (*m/z* 133, 107, and 81) that were not detected for TRA (see Fig. S4). These product ions offer the possibility of additional, selective MRM transitions for ODV, albeit with relatively poor limits of detection and quantitation (LOD and LOQ, respectively) owing to their low signal intensities. We confirmed these as useful MRM transitions using a reverse-phase LC method capable of chromatographically resolving ODV and TRA (see Table S1; LC Method A, Table S3 and Fig. S5) and were able to improve the LOD somewhat by employing EPI scan mode but could not find a similar solution for quantifying TRA. Consequently, the approach of using unique CID fragments alone is inadequate for confident trace environmental analysis of these compounds, and exploration of alternative separation and filtering methods offered by IMS is desirable.

3.2. Chiral LC-MS^2 analysis

Reverse-phase LC-MS^2 can be used to analyze the racemic concentrations of ODV and TRA, but this approach does not provide information about enantiomer abundances. To address enantiomer concentrations, we introduced chiral LC to our workflow and, although we could separate the enantiomers of ODV and TRA, we found that the (*R*,*R*)-TRA and (*S*)-ODV species co-elute (see Fig. 1). Using the unique fragments of ODV (*i.e.*, *m/z* 133, 107, and 81), we can selectively measure (*S*)-ODV and (*R*)-ODV, but can only determine (*R*,*R*)-TRA concentration *via* subsequent peak subtraction (which introduces additional uncertainty to the result). To overcome this limitation, we decided to introduce IMS, testing both DMS and TWIMS as methods that could potentially address this co-elution.

Using TWIMS, we measured CCS values of Ω_{N2}(ODV) = 166.0 ± 0.5 Å^2 and Ω_{N2}(TRA) = 160.9 ± 0.3 Å^2, both of which are in excellent agreement with values measured by Vincent *et al.* and values computed using MobCal-MPI 2.0 (see Table S4).[53] The ΔCCS ≈ 3.1% is expected to be near-threshold for the resolution of two isomeric compounds *via* TWIMS as implemented on the Waters Synapt G2-Si.[54] This was confirmed upon infusion of a mixture of ODV and TRA, where the ODV shoulder was observed to exhibit a longer drift time of the TRA peak (see Fig. S6). Because ODV and TRA could not be baseline resolved *via* TWIMS, we decided that implementing a chiral LC × TWIMS analysis would not be useful and instead chose to explore DMS as an option for our second separation dimension.

3.3. DMS-MS analysis

A DMS cell temperature of DT = 150 °C and 1.5 mol% of IPA modifier enabled baseline resolution at SV = 3500 V. Note that lower DT settings can be used to further improve resolution, or to maintain similar baseline resolution at a lower SV, as has been observed in other works.[24] The conditions used here

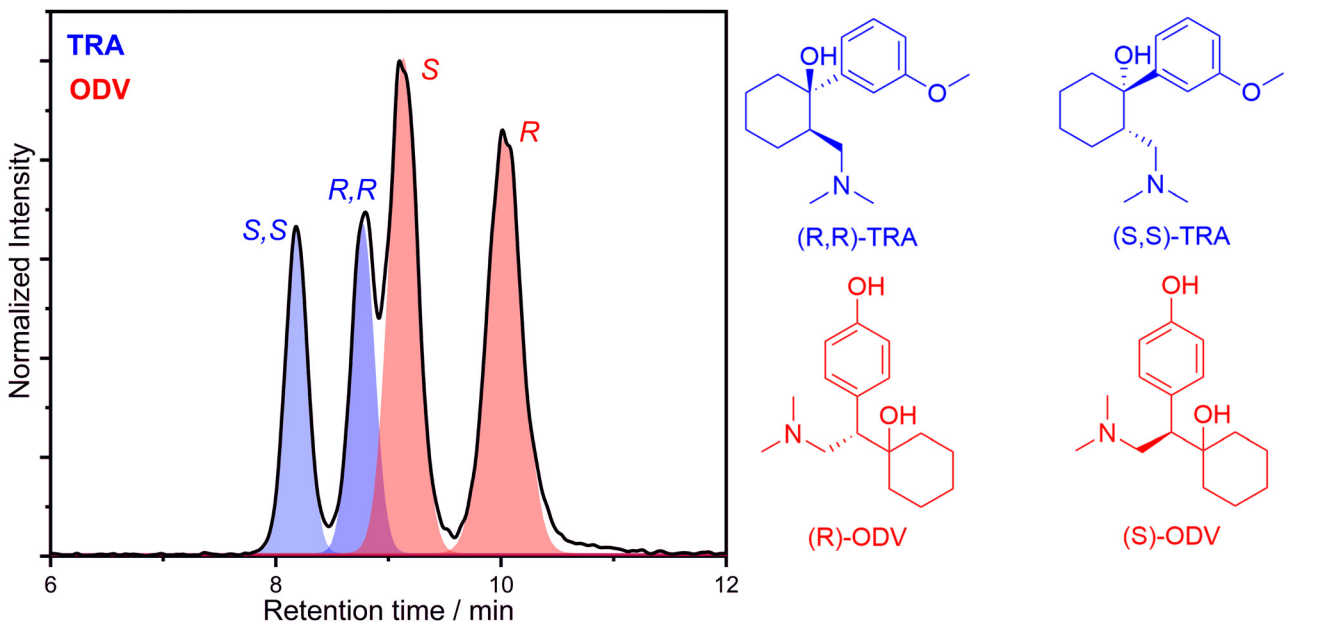

Fig. 1 Chromatogram of ODV and TRA present in a wastewater influent extract sample when analyzed by chiral LC-MS^2 and employing the *m/z* 264 → 58 MRM transition.

were tuned from Werres and coworkers, where the partial separation of ODV and TRA was achieved using DMS operating at DT = 225 °C and SV = 3500 V in an IPA-modified environment.[19] Care should be taken when employing DT < 150 °C for two-dimensional LC × DMS workflows, though, because the relatively high ESI source temperature required for the LC source can impact the DMS cell temperature, potentially introducing additional heating and a temperature gradient within the DMS cell and affect dispersion behaviours. Moreover, for low vapor pressure solvents, low DMS cell temperatures could lead to condensation on the DMS electrodes, which can potentially impact instrument electrical stability and operation.

To evaluate separation of ODV and TRA, the *m*/*z* 264 → 58 MRM transition was employed. When introducing 1.5 mol% IPA as a modifier, DR gas was not required to yield baseline resolution of the isomers. Similar optimization of other solvent modifiers (*i.e.*, acetonitrile, ethyl acetate, and methanol) also yielded baseline separation of ODV and TRA, but these other solvents required an increased DR gas flow. In the case of acetone, introducing 25 psi of DR gas was still not sufficient for baseline separation at DT 150 °C. Table 1 provides an overview of the solvent modifiers tested, reporting the resolution of the ODV and TRA ionogram features under optimized DR gas conditions, and the approximate loss of sensitivity by employing DR gas. These sensitivity losses, which stem from ion diffusion during the longer residence times when employing DR gas, negatively impact the LOD/LOQ. Because baseline separation was achieved using IPA modifier without the need for increased DR, we chose to employ IPA-modified conditions for further method development. Fig. 2A shows the dispersion curves measured for a mixture of ODV and TRA when employing the IPA-modified environment at DT = 150 °C. At SV 3000 V, the features begin to appear as separate features. At SV ≥ 3500 V, the two isomers are spatially resolved *via* DMS. Fig. 2B shows the ionogram recorded at SV = 3750 V (Resolution = 2.8, refer to eqn (S2)), which corresponds to the green highlighted area in panel A. The more substantial deflection of ODV in CV-space indicates that it clusters more strongly

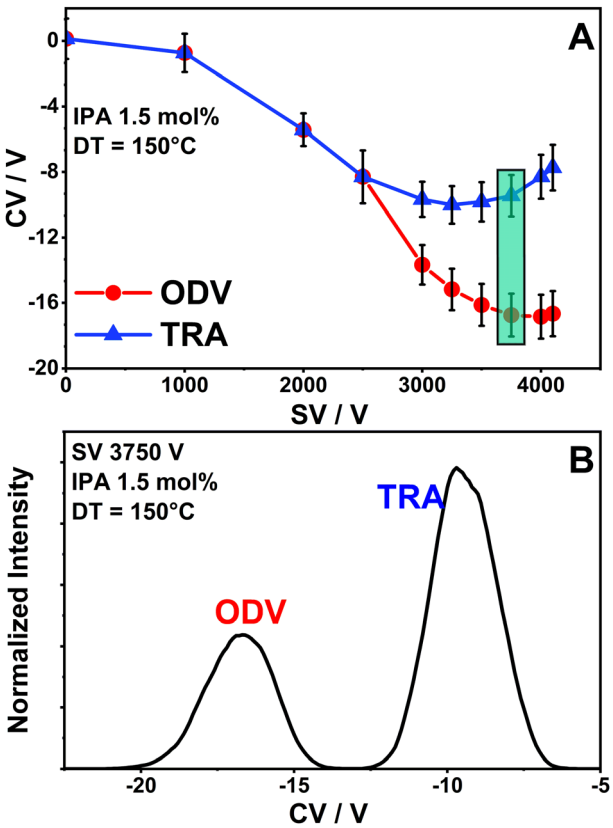

Fig. 2 (A) DMS dispersion curves for protonated ODV and TRA in 1.5 mol% IPA in a N_2 carrier at DT = 150 °C. The SV for optimal separation is highlighted in green, and the corresponding ionogram is plotted in panel B. Error bars correspond to a HWHM of the ionogram feature. (B) The ionogram measured for a mixture of ODV and TRA at SV = 3750 V.

Table 1 Overview of the optimal conditions for resolution of ODV and TRA for a variety of solvent-modified environments. Solvent modifiers were introduced at 1.5 mol% and DT = 150 °C. Three DR gas settings were tested (0, 10 and 25 psi) for each modified environment. The % signal loss compares the difference between ion signals with and without DR gas relative to the intensity without DR gas, where N/A denotes that no DR gas was required for baseline resolution

Solvent modifier used	DR gas pressure setting/psi	SV/V	Resolution	% TRA signal loss	% ODV signal loss
Methanol	25	4100	1.9	~90%	~85%
Acetonitrile	10	3000	1.8	~70%	~40%
Acetone	25	3500	<1.5[a]	~90%	~90%
Ethyl acetate	10	3500	1.6	~65%	~20%
Isopropanol	0	3750	2.8	N/A	N/A

[a] Ionogram peaks were not baseline separated at these conditions.

with IPA than does TRA. To test this hypothesis computationally, we conducted *in silico* experiments to assess the binding energies (BE) of IPA with the analyte molecules. For single solvent clusters, ion-solvent BEs are approximately equal. However, clusters containing two IPA molecules, the BE(ODV) > BE(TRA) (see Table S5). This result suggests that ODV forms larger clusters with IPA and that these clusters persist longer into the high-field portion of the SV waveform than do those containing TRA, driving a larger differential mobility for ODV (as is observed experimentally).

3.4. Two-dimensional chiral LC × DMS-MS^2

When combining the orthogonal chiral LC and DMS separation dimensions, each enantiomer was monitored throughout the chiral LC run using identical parent-to-product MRM transitions (*m*/*z* 264 → 58), while specifying the unique CVs for TRA and ODV. As observed in previous work, the integration of LC and DMS-MS^2 systems can cause small shifts in CV values due to the introduction of mobile phase solvent vapour into the carrier gas. Thus, daily checks of peak centroid values are required for consistency.[32] To investigate these potential shifts in DMS behaviour compared to direct infusion experiments, a

mixture of ODV and TRA was t-infused with the chiral LC mobile phase into the DMS. The observed CV centroids for each isomer were then employed in our MRM table. Additional technical details are provided in the SI. This methodology was used to generate the two-dimensional heatmap of the separation space shown in Fig. 3, which employed a wastewater influent sample wastewater extracted *via* SPE. The corresponding liquid chromatogram observed in each DMS CV channel is shown to the right in Fig. 3, demonstrating the complete separation of each set of enantiomers in the chiral LC × DMS space. Example MRM tables used for LC-MS^2 analysis (Table S6) and LC × DMS-MS^2 (Table S7) are provided in the SI.

To determine the method LOQ, we assessed signal-to-noise (S/N) ratios for ODV and TRA using the Analyst software. A window of width 1-minute prior to elution of the first enantiomer was employed to assess noise during acquisition of calibration curve data using internal standards (TRA^{13}C-D_3 and ODV-D_6). Peak integration was performed using the Quantitation Method and the Quantitation Wizard modules in the Analyst software. Using LOQ = 10 × S/N, we determined values of 5.0 ng mL^{-1} for the enantiomers of ODV and estimated 0.67 ng mL^{-1} for the enantiomers of TRA. The difference between the instrumental LOQs and the approach of determining S/N ratios is provided in the SI, along with the S/N ratios observed for low concentration calibration points used for instrumental LOQ assignments (Table S8). To test method quantitation, we compared the results of our method against the results of reverse-phase LC-MS^2 measurements. Because reverse-phase LC cannot resolve enantiomers, peak areas for ODV and TRA represent the sum of their enantiomeric pairs. Thus, for comparison, it was necessary to sum the (*S*)-ODV and (*R*)-ODV features and the (*S*,*S*)-TRA and (*R*,*R*)-TRA features measured using the chiral LC × DMS-MS^2 method. Fig. 4A shows a comparison of (*S*)-ODV and (*R*)-ODV concentrations as measured using the chiral LC × DMS-MS^2 method with the ODV concentration measured using reverse-phase LC-MS^2 for influent samples taken on six different days (within an 8-day period) at a municipal wastewater treatment plant in Ontario. Fig. 4B shows a similar plot for (*S*,*S*)-TRA and (*R*,*R*)-TRA concentrations measured using the chiral LC × DMS-MS^2 method and total TRA concentration measured using reverse-phase LC-MS^2. For each analyte, a nine-point calibration curve was prepared ranging from 1–300 ng mL^{-1}, where the ratio of the analyte peak area and the corresponding internal standard peak area was plotted against the analyte concentration.

In both cases, the total analyte concentration determined using the chiral LC × DMS-MS^2 method is in excellent agreement with that determined *via* reverse-phase LC-MS^2. For the 6-day period, we determined a total ODV concentration of 1170 ± 50 ng L^{-1} *via* LC × DMS-MS^2 and 1210 ± 70 ng L^{-1} *via* LC-MS^2, which are statistically identical (t-test; α = 0.05, *p*-value = 0.26). Similarly, for TRA, we determined statistically identical total concentrations of 72 ± 6 ng L^{-1} *via* LC × DMS-MS^2 and 75 ± 6 ng L^{-1} *via* LC-MS^2 (t-test; α = 0.05, *p*-value = 0.47).

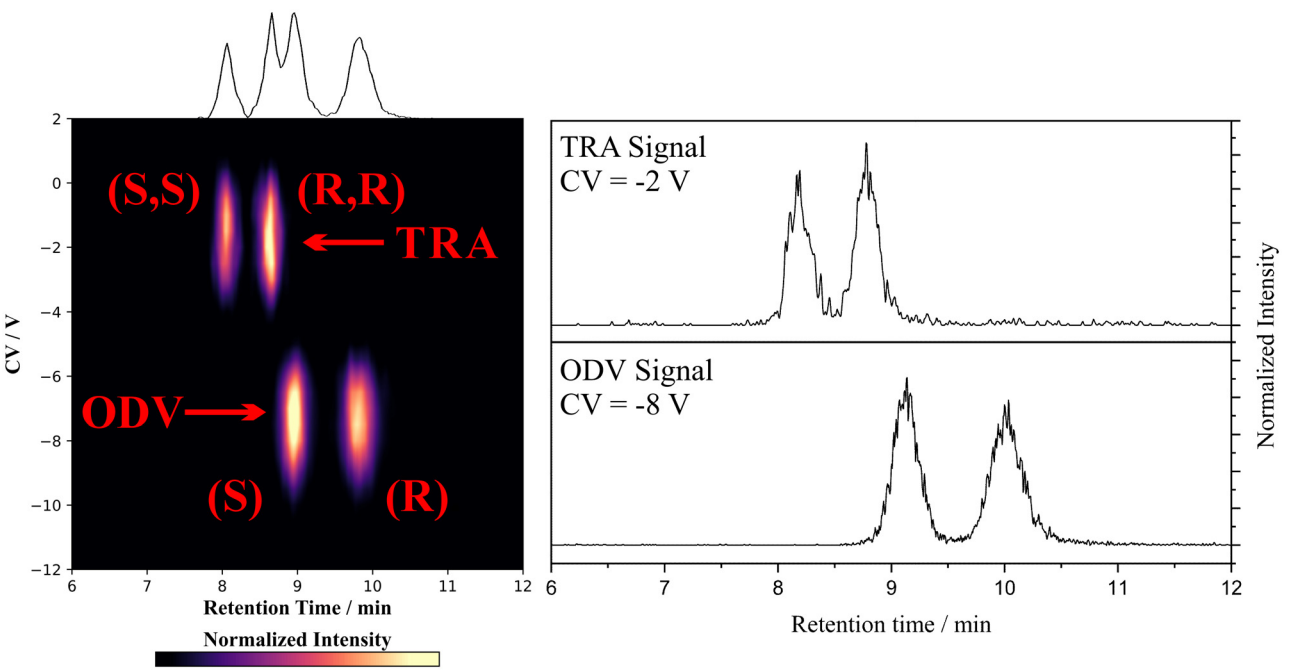

Fig. 3 (Left) Two-dimensional chiral LC × DMS-MS^2 heatmap of ODV and TRA detected in influent from an Ontario wastewater treatment plant. Both isomers were monitored *via* the *m*/*z* 264 → 58 transition. (Right) The chiral LC chromatograms recorded for TRA and ODV in their respective DMS CV channels.

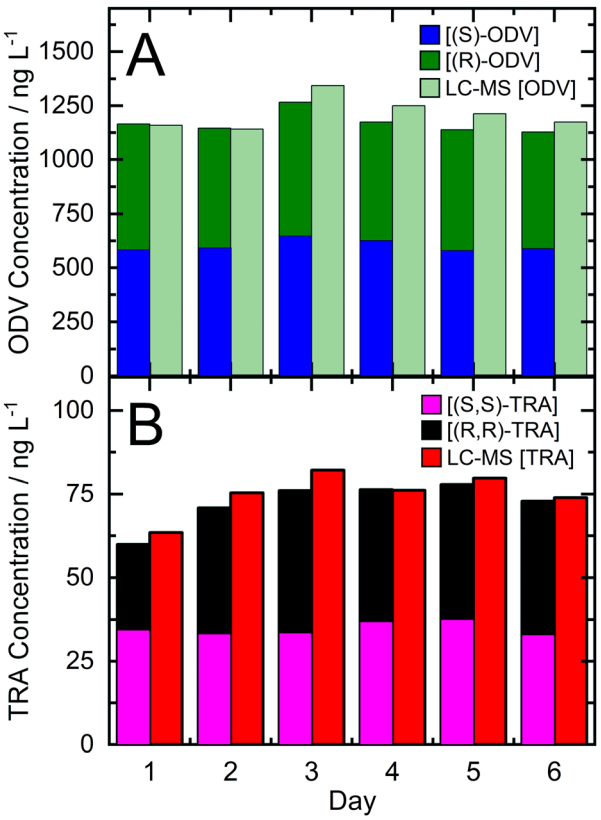

Fig. 4 Concentrations of (A) ODV and (B) TRA determined for six Ontario municipal wastewater (influent) samples from the same treatment plant using LC-MS and chiral LC × DMS-MS^2.

4. Conclusion

By incorporating DMS into a chiral LC-MS^2 workflow, we could resolve (*S*) and (*R*) enantiomers of ODV and separate them from the (*S*,*S*) and (*R*,*R*) enantiomers of TRA in wastewater samples. Several different solvent modifiers enabled baseline separation of ODV and TRA in CV-space, but employing 1.5 mol% IPA at DT = 150 °C facilitates separation (Resolution = 2.8) without the need of resolving gas, preserving ion signal and yielding relatively low LOQs. DMS dispersion curves indicate that ODV clusters more strongly with IPA than TRA binds with IPA, a result that is supported by quantum chemical calculations. Although we did not observe significant ion fragmentation at high SV, one could potentially refine our method by reducing SV and varying gas temperature or modifier concentration to tune dynamic clustering.

The two-dimensional chiral LC × DMS-MS^2 method yielded LOQs of 5.0 ng mL^{-1} for (*S*)-ODV/(*R*)-ODV and an estimated LOQ of 0.67 ng mL^{-1} for (*S*,*S*)-TRA/(*R*,*R*)-TRA. These LOQs are substantially lower than the concentrations of ODV and TRA that we quantified in extracts from municipal wastewater influent samples. Comparing six measurements taken over an eight-day period at the same wastewater treatment facility, it is shown that the sum of the enantiomeric concentrations determined using the chiral LC × DMS-MS^2 method ([ODV] = 1170 ± 50 ng L^{-1}, [TRA] = 72 ± 6 ng L^{-1}) were statistically identical to the total concentrations determined *via* LC-MS^2 ([ODV] = 1210 ± 70 ng L^{-1}, [TRA] = 75 ± 6 ng L^{-1}). This result inspires confidence that the chiral LC × DMS-MS^2 workflow can separate and accurately quantify individual enantiomers. This technique could be useful for studying the various enantiomers of isomer sets such as morphine (5 chiral centers), hydromorphone (4 chiral centers), and norcodeine (5 chiral centers), which have chemical formula $C_{17}H_{18}NO_3$, or the codeine/hydrocodone isomer pair (5 and 4 chiral centers, respectively), which has chemical formula $C_{18}H_{21}NO_3$. Accurate quantification of enantiomers of chemical systems such as these could enable studies of, for example, enantiomeric bioaccumulation and toxicology of environmental pharmaceuticals in wildlife and humans.

Author contributions

A. D. M. and R. V. contributed equally to this work. A. Dawson McLachlan investigation, methodology, visualization, writing – original draft; Rashne Vakharia investigation, methodology, writing – review & editing; Emir Nazdrajić conceptualization, investigation, writing – review & editing; Diana M. Cárdenas-Soracá conceptualization, writing – review & editing; Leslie M. Bragg project administration, resources, writing – review & editing; Mark R. Servos conceptualization, funding acquisition, project administration, supervision, writing – review & editing; W. Scott Hopkins conceptualization, supervision, writing – review & editing.

Conflicts of interest

There are no conflicts to declare.

Data availability

The data for this article, including the energy calculations for each conformer of each isomer and the energy calculations required for binding energy calculations are openly available in ioChem-BD at https://doi.org/10.19061/iochem-bd-6-617.

Supplementary information (SI): details concerning experimental details of the enhanced product ion scan validation, CV verification, determination of signal-to-noise ratios, determination of resolution, and experimental details of LC-MS, LC × DMS-MS^2, and TWIMS. See DOI: https://doi.org/10.1039/d6an00119j.

Ref. 45 and 53 are cited in the SI and the article, and ref. 55 is cited in the SI.

Acknowledgements

This project was made possible due to funding from NSERC Discovery (#RGPIN2017-03816), Grants and Contributions

from Environment and Climate Change Canada (ECCC) (#GCXE25S081), NSERC Alliance with the Ontario Ministry of Environment, Conservation and Parks (# ALLRP 597566-24) and Global Water Futures – Observatories (#42687).

References

1 A. R. Ribeiro, P. M. L. Castro and M. E. Tiritan, Chiral Pharmaceuticals in the Environment, *Environ. Chem. Lett.*, 2012, **10**(3), 239–253, DOI: 10.1007/s10311-011-0352-0.
2 V. K. Vashistha, Detection and Remediation of Chiral Pharmaceuticals from Wastewater: A Review, *Chirality*, 2022, **34**(6), 833–847, DOI: 10.1002/chir.23437.
3 J. K. Stanley and B. W. Brooks, Perspectives on Ecological Risk Assessment of Chiral Compounds, *Integr. Environ. Assess. Manage.*, 2009, **5**(3), 364–373, DOI: 10.1897/IEAM_2008-076.1.
4 K. Kümmerer, Pharmaceuticals in the Environment, *Annu. Rev. Environ. Resour.*, 2010, **35**(1), 57–75, DOI: 10.1146/annurev-environ-052809-161223.
5 M. Arenas, J. Martín, J. L. Santos, I. Aparicio and E. Alonso, Enantioselective Behavior of Environmental Chiral Pollutants: A Comprehensive Review, *Crit. Rev. Environ. Sci. Technol.*, 2022, **52**(17), 2995–3034, DOI: 10.1080/10643389.2021.1900764.
6 P.-H. Nguyen, H. He and L. A. Chuong, Chiral Drugs. An Overview, *Int. J. Biomed. Sci.*, 2006, **2**(2), 85–100, DOI: 10.59566/IJBS.2006.2085.
7 L. Dutta, S. I. Ahmad, S. K. Mukherjee, S. Mishra, A. Khuroo and T. Monif, Liquid Chromatography Tandem Mass Spectrometry Method for the Simultaneous Stereoselective Determination of Venlafaxine and Its Major Metabolite, O-Desmethylvenlafaxine, in Human Plasma, *Biomed. Chromatogr.*, 2013, **27**(5), 622–635, DOI: 10.1002/bmc.2837.
8 W. A. Thompson, Z. Shvartsburd and M. M. Vijayan, The Antidepressant Venlafaxine Perturbs Cardiac Development and Function in Larval Zebrafish, *Aquat. Toxicol.*, 2022, **242**, 106041, DOI: 10.1016/j.aquatox.2021.106041.
9 Q. Chen, S. Gu, Y. Lan, J. Xu, W. Lin, Y. Qin and Y. Ren, Study on the Developmental, Behavioral Toxicity, and Toxicological Mechanism of the Antidepressant Drug Venlafaxine and Its Active Metabolites in Zebrafish, *Environ. Toxicol. Chem.*, 2025, **44**(2), 552–562, DOI: 10.1093/etojnl/vgae055.
10 P. Rodrigues, L. Guimarães, A. P. Carvalho, L. Oliva-Teles and V. Carbamazepine, Tramadol, and Their Main Metabolites: Toxicological Effects on Zebrafish Embryos and Larvae, *J. Hazard. Mater.*, 2023, **448**, 130909, DOI: 10.1016/j.jhazmat.2023.130909.
11 I. Agranat and I. D'Acquarica, Chiral Switches of Tramadol Hydrochloride, a Potential Psychedelic Drug—Past and Future, *ACS Med. Chem. Lett.*, 2024, **15**(9), 1409–1416, DOI: 10.1021/acsmedchemlett.4c00322.
12 I. D'Acquarica and I. Agranat, A Call to Develop Tramadol Enantiomer for Overcoming the Tramadol Crisis by Reducing Addiction, *Future Med. Chem.*, 2025, **17**(5), 505–507, DOI: 10.1080/17568919.2025.2463314.
13 J. M. Peña-Herrera, N. Montemurro, D. Barceló and S. Pérez, Development and Validation of an Analytical Method for Determination of Pharmaceuticals in Fish Muscle Based on QuEChERS Extraction and SWATH Acquisition Using LC-QTOF-MS/MS System, *Talanta*, 2019, **199**, 370–379, DOI: 10.1016/j.talanta.2019.01.119.
14 C. Aydoğan, B. B. Çakan and A. Ali, A Review on the Analysis of Chiral Molecules as Disease Biomarkers by LC/MS, *Biomed. Chromatogr.*, 2025, **39**(1), e6044, DOI: 10.1002/bmc.6044.
15 M. Arenas, J. Martín, J. L. Santos, I. Aparicio and E. Alonso, Automatised Online SPE-LC-MS/MS Method for the Enantioselective Determination of Chiral β-Blockers and Antidepressants in Wastewater, *Anal. Chim. Acta*, 2025, **1361**, 344152, DOI: 10.1016/j.aca.2025.344152.
16 S. Kowalczyk, *Determination of the Accumulation of Chiral Pharmaceuticals (Venlafaxine and O-Desmethylvenlafaxine) in Rainbow Darters (Etheostoma Caeruleum)*, University of Waterloo, 2025. https://hdl.handle.net/10012/21406.
17 L. Li, R. Zhou, H. Xie, G. Li, Z. Xu, M. Liu and W. Gao, Chiral Separation and Determination of Multiple Organophosphorus Pesticide Enantiomers in Soil Based on Cellulose-Based Chiral Column by LC–MS/MS, *J. Sep. Sci.*, 2025, **48**(2), e70100, DOI: 10.1002/jssc.70100.
18 M. Hefnawy, A. Al-Majed, H. Alrabiah, N. Algrain, M. Mohammed and Y. B. Jardan, Rapid and Sensitive LC-MS/MS Method for the Enantioanalysis of Verapamil in Rat Plasma Using Superficially Porous Silica Isopropyl-Cyclofructan 6 Chiral Stationary Phase after SPE: Application to a Stereoselective Pharmacokinetic Study, *J. Pharm. Biomed. Anal.*, 2021, **201**, 114108, DOI: 10.1016/j.jpba.2021.114108.
19 T. Werres, J. Leonhardt, M. Jäger and T. Teutenberg, Critical Comparison of Liquid Chromatography Coupled to Mass Spectrometry and Three Different Ion Mobility Spectrometry Systems on Their Separation Capability for Small Isomeric Compounds, *Chromatographia*, 2019, **82**(1), 251–260, DOI: 10.1007/s10337-018-3640-z.
20 C. Ieritano, A. N. Fry, J. N. Dodds, E. S. Baker and W. S. Hopkins, Three Candidates, Two Peaks: Addressing Conflicting Assignments of Fentanyl Protomers with DMS-UVPD, *J. Am. Soc. Mass Spectrom.*, 2025, **36**(9), 1889–1901, DOI: 10.1021/jasms.5c00130.
21 C. Ieritano, P. Thomas and W. S. Hopkins, Argentination: A Silver Bullet for Cannabinoid Separation by Differential Mobility Spectrometry, *Anal. Chem.*, 2023, **95**(22), 8668–8678, DOI: 10.1021/acs.analchem.3c01241.
22 C. Ieritano and W. S. Hopkins, The Hitchhiker's Guide to Dynamic Ion–Solvent Clustering: Applications in Differential Ion Mobility Spectrometry, *Phys. Chem. Chem. Phys.*, 2022, **24**(35), 20594–20615, DOI: 10.1039/D2CP02540J.

23 J. L. Campbell, J. C. Y. Le Blanc and B. B. Schneider, Probing Electrospray Ionization Dynamics Using Differential Mobility Spectrometry: The Curious Case of 4-Aminobenzoic Acid, *Anal. Chem.*, 2012, **84**(18), 7857–7864, DOI: 10.1021/ac301529w.

24 N. Mashmoushi, J. L. Campbell, R. di Lorenzo and W. S. Hopkins, Rapid Separation of Cannabinoid Isomer Sets Using Differential Mobility Spectrometry and Mass Spectrometry, *Analyst*, 2022, **147**, 2198, DOI: 10.1039/d1an02327f.

25 C. Ieritano, D. Rickert, J. Featherstone, J. F. Honek, J. L. Campbell, J. C. Y. Le Blanc, B. B. Schneider and W. S. Hopkins, The Charge-State and Structural Stability of Peptides Conferred by Microsolvating Environments in Differential Mobility Spectrometry, *J. Am. Soc. Mass Spectrom.*, 2021, **32**, 956–968, DOI: 10.1021/jasms.0c00469%3Frel=cite-as&ref=PDF&jav=VoR.

26 B. B. Schneider, E. G. Nazarov, F. Londry, P. Vouros and T. R. Covey, Differential Mobility Spectrometry/Mass Spectrometry History, Theory, Design Optimization, Simulations, and Applications, *Mass Spectrom. Rev.*, 2016, **35**(6), 687–737, DOI: 10.1002/mas.21453.

27 C. Ieritano and W. S. Hopkins, The Hitchhiker's Guide to Dynamic Ion–Solvent Clustering: Applications in Differential Ion Mobility Spectrometry, *Phys. Chem. Chem. Phys.*, 2022, **24**(35), 20594–20615, DOI: 10.1039/D2CP02540J.

28 W. Jin, M. Jarvis, M. Star-Weinstock and M. Altemus, A Sensitive and Selective LC-Differential Mobility-Mass Spectrometric Analysis of Allopregnanolone and Pregnanolone in Human Plasma, *Anal. Bioanal. Chem.*, 2013, **405**(29), 9497–9508, DOI: 10.1007/s00216-013-7391-2.

29 Y. Chai, S. K. G. Grebe and A. Maus, Improving LC-MS/MS Measurements of Steroids with Differential Mobility Spectrometry, *J. Mass Spectrom. Adv. Clin. Lab*, 2023, **30**, 30–37, DOI: 10.1016/j.jmsacl.2023.10.001.

30 C. Jacquet and G. Hopfgartner, Microflow Liquid Chromatography Coupled to Mass Spectrometry (μLC–MS) Workflow for O-Glycopeptides Isomers Analysis Combining Differential Mobility Spectrometry and Collision Induced and Electron Capture Dissociation, *J. Am. Soc. Mass Spectrom.*, 2022, **33**(4), 688–694, DOI: 10.1021/jasms.1c00381.

31 L. Ekmekciu and G. Hopfgartner, Liquid Chromatography and Differential Mobility Spectrometry—Data-Independent Mass Spectrometry for Comprehensive Multidimensional Separations in Metabolomics, *Anal. Bioanal. Chem.*, 2023, **415**(10), 1905–1915, DOI: 10.1007/s00216-023-04602-0.

32 C. R. M. Ryan, E. Nazdrajić, J. L. Campbell, K. Y. Bell and W. S. Hopkins, Two-Dimensional LC × DMS Analysis of 34 PFAS Compounds, *Anal. Chem.*, 2025, **97**(38), 21050–21059, DOI: 10.1021/acs.analchem.5c04119.

33 M. F. Cifuentes Girard, P. Knight and G. Hopfgartner, High-Throughput Liquid Chromatography-Vacuum Differential Mobility Spectrometry-Mass Spectrometry for the Analysis of Isomeric Drugs of Abuse in Human Urine, *Drug Test. Anal.*, 2025, **17**(6), 751–760, DOI: 10.1002/dta.3778.

34 D. M. Cárdenas-Soracá, S. Salic, L. Warkentin, C. Chong, P. A. Ortiz-Suarez, R. Vakharia, L. Bragg and M. R. Servos, Unraveling Matrix Effects: A Study on Drugs of Abuse in Wastewater Samples from Southern Ontario, Canada, *ACS EST Water*, 2025, **5**(8), 4423–4434, DOI: 10.1021/acsestwater.5c00092.

35 P. Pracht, S. Grimme, C. Bannwarth, F. Bohle, S. Ehlert, G. Feldmann, J. Gorges, M. Müller, T. Neudecker, C. Plett, S. Spicher, P. Steinbach, P. A. Wesołowski and F. Zeller, CREST—A Program for the Exploration of Low-Energy Molecular Chemical Space, *J. Chem. Phys.*, 2024, **160**(11), 114110, DOI: 10.1063/5.0197592.

36 S. Grimme, J. Antony, S. Ehrlich and H. Krieg, A Consistent and Accurate Ab Initio Parametrization of Density Functional Dispersion Correction (DFT-D) for the 94 Elements H-Pu, *J. Chem. Phys.*, 2010, **132**(15), 154104, DOI: 10.1063/1.3382344.

37 F. Weigend, Accurate Coulomb-Fitting Basis Sets for H to Rn, *Phys. Chem. Chem. Phys.*, 2006, **8**(9), 1057–1065, DOI: 10.1039/B515623H.

38 B. Helmich-Paris, B. de Souza, F. Neese and R. Izsák, An Improved Chain of Spheres for Exchange Algorithm, *J. Chem. Phys.*, 2021, **155**(10), 104109, DOI: 10.1063/5.0058766.

39 F. Neese, An Improvement of the Resolution of the Identity Approximation for the Formation of the Coulomb Matrix, *J. Comput. Chem.*, 2003, **24**(14), 1740–1747, DOI: 10.1002/jcc.10318.

40 R. Izsák and F. Neese, An Overlap Fitted Chain of Spheres Exchange Method, *J. Chem. Phys.*, 2011, **135**(14), 144105, DOI: 10.1063/1.3646921.

41 F. Weigend and R. Ahlrichs, Balanced Basis Sets of Split Valence, Triple Zeta Valence and Quadruple Zeta Valence Quality for H to Rn: Design and Assessment of Accuracy, *Phys. Chem. Chem. Phys.*, 2005, **7**(18), 3297–3305, DOI: 10.1039/B508541A.

42 D. Bykov, T. Petrenko, R. Izsák, S. Kossmann, U. Becker, E. Valeev and F. Neese, Efficient Implementation of the Analytic Second Derivatives of Hartree–Fock and Hybrid DFT Energies: A Detailed Analysis of Different Approximations, *Mol. Phys.*, 2015, **113**(13–14), 1961–1977, DOI: 10.1080/00268976.2015.1025114.

43 R. Izsák, F. Neese and W. Klopper, Robust Fitting Techniques in the Chain of Spheres Approximation to the Fock Exchange: The Role of the Complementary Space, *J. Chem. Phys.*, 2013, **139**(9), 094111, DOI: 10.1063/1.4819264.

44 F. Weigend and R. Ahlrichs, Balanced Basis Sets of Split Valence, Triple Zeta Valence and Quadruple Zeta Valence Quality for H to Rn: Design and Assessment of Accuracy, *Phys. Chem. Chem. Phys.*, 2005, **7**(18), 3297–3305, DOI: 10.1039/B508541A.

45 A. Haack, C. Ieritano and W. S. Hopkins, MobCal-MPI 2.0: An Accurate and Parallelized Package for Calculating Field-

Dependent Collision Cross Sections and Ion Mobilities, *Analyst*, 2023, **148**, 3257–3273, DOI: 10.1039/d3an00545c.
46 C. Ieritano, J. Crouse, J. L. Campbell and W. S. Hopkins, A Parallelized Molecular Collision Cross Section Package with Optimized Accuracy and Efficiency, *Analyst*, 2019, **144**(5), 1660–1670, DOI: 10.1039/C8AN02150C.
47 C. Ieritano, HopkinsLaboratory/MobCal-MPI: MobCal-MPI 2.0.3, 2024. DOI: 10.5281/zenodo.11426097.
48 F. Neese, Software Update: The ORCA Program System—Version 5.0, *Wiley Interdiscip. Rev.: Comput. Mol. Sci.*, 2022, **12**(5), e1606, DOI: 10.1002/wcms.1606.
49 F. Neese, The ORCA Program System, *Wiley Interdiscip. Rev.: Comput. Mol. Sci.*, 2012, **2**(1), 73–78, DOI: 10.1002/wcms.81.
50 F. Neese, Software Update: The ORCA Program System, Version 4.0, *Wiley Interdiscip. Rev.: Comput. Mol. Sci.*, 2018, **8**(1), e1327, DOI: 10.1002/wcms.1327.
51 F. Neese, F. Wennmohs, U. Becker and C. Riplinger, The ORCA Quantum Chemistry Program Package, *J. Chem. Phys.*, 2020, **152**(22), 224108, DOI: 10.1063/5.0004608.
52 C. Ieritano, *PodPals*, 2024. DOI: 10.5281/zenodo.11583238.
53 E. Vincent, J. Dodds and E. Baker, LC-IMS-CID-MS Library for Antidepressant and Antidepressant Metabolites (Updated August 2025), 2025. DOI: 10.5281/zenodo.16928332.
54 J. N. Dodds, J. C. May and J. A. McLean, Correlating Resolving Power, Resolution, and Collision Cross Section: Unifying Cross-Platform Assessment of Separation Efficiency in Ion Mobility Spectrometry, *Anal. Chem.*, 2017, **89**(22), 12176–12184, DOI: 10.1021/acs.analchem.7b02827.
55 B. T. Ruotolo, J. L. P. Benesch, A. M. Sandercock, S.-J. Hyung and C. V. Robinson, Ion Mobility–Mass Spectrometry Analysis of Large Protein Complexes, *Nat. Protoc.*, 2008, **3**(7), 1139–1152, DOI: 10.1038/nprot.2008.78.